



Article

Remote Seismoacoustic Monitoring of Tropical Cyclones in the Sea of Japan

Grigory Dolgikh ¹, Stanislav Dolgikh ^{1,*}, Vladimir Chupin ¹, Aleksandr Davydov ¹
and Aleksandr Mishakov ²

¹ V.I. Il'ichev Pacific Oceanological Institute, Far Eastern Branch Russian Academy of Sciences, 690041 Vladivostok, Russia; chupin@poi.dvo.ru (V.C.)

² Department of Mathematics, Institute of Mathematics and Computer Technologies, Far Eastern Federal University, 690922 Vladivostok, Russia

* Correspondence: sdolgikh@poi.dvo.ru

Abstract: In the course of processing and analysing data from a two-coordinate laser strainmeter, obtained during the propagation of the Hagupit typhoon over the Sea of Japan, we researched the possibility of sensing the direction of tropical cyclones/typhoons and also tracking their movements. We tackled the set of problems on the basis of further development of the technology for sensing the direction of primary and secondary microseisms' generation zones, the "voice of the sea" microseisms, and clarifying the connection between their formation zones and movement of tropical cyclones. In our work, we identified the formation zones of primary and secondary microseisms, which were registered by the two-coordinate laser strainmeter. We established that, from the registered microseisms, we could determine the main characteristics of wind waves generated by a typhoon, but we could not identify its location. By processing the two-coordinate laser strainmeter data in the range of the "voice of the sea" microseisms, we established the possibility of sensing the direction of the "voice of the sea" microseisms' formation zones, which are associated with zones of the highest energy capacity of typhoons, and this allowed us to tracking the direction of the typhoons' movement.

Keywords: typhoon; tropical cyclone; primary and secondary microseisms; "voice of the sea"; laser strainmeter



Citation: Dolgikh, G.; Dolgikh, S.; Chupin, V.; Davydov, A.; Mishakov, A. Remote Seismoacoustic Monitoring of Tropical Cyclones in the Sea of Japan. *Remote Sens.* **2023**, *15*, 1707. <https://doi.org/10.3390/rs15061707>

Academic Editors: Korak Saha and Zhankun Wang

Received: 17 February 2023

Revised: 20 March 2023

Accepted: 20 March 2023

Published: 22 March 2023



Copyright: © 2023 by the authors. Licensee MDPI, Basel, Switzerland. This article is an open access article distributed under the terms and conditions of the Creative Commons Attribution (CC BY) license (<https://creativecommons.org/licenses/by/4.0/>).

1. Introduction

Tropical cyclones/typhoons are among the most powerful catastrophic processes/phenomena of the Earth, and they bring colossal economic damage to mankind. Moreover, according to the total annual energy capacity, they are the most powerful phenomena of the Earth. It is clear that, when forecasting a typhoons' origin, continuous real-time monitoring of their behaviour is essential to reduce their possible impact on the results of human activity and to minimize economic losses. For this purpose, various contact and remote methods have been developed in the world, which solve monitoring problems with varying degrees of success. At present, remote methods include, first of all, satellite monitoring methods, which, along with a seemingly obvious advantage, have a number of disadvantages. One of the main drawbacks is the necessity to correct the obtained observations data with the data of stationary complexes. It especially relates to the data obtained for the shelf coastal regions, where multiscale dynamic processes of geosphere fields are developed, which influence one another. Together with satellite methods, remote methods include parametric methods, which are focused on studying the secondary manifestations of typhoons, their origins, dynamics, and transformation. If wind and precipitation relate to the primary manifestations of typhoons, their secondary manifestations should include: (1) wind waves, which result from wind impact on extended water areas; (2) primary and secondary microseisms, which result from the interaction of progressive and standing wind waves, respectively, with the seabed; (3) infrasound signals of the "voice of the sea", which

were first discovered by V.V. Shuleikin in 1935; (4) signals from other geosphere fields. In this work, we will focus on studying the possibilities of using some of the secondary manifestations of typhoons for their remote monitoring, which include primary, secondary, and “voice of the sea” microseisms.

Paper [1] states that progressive and standing sea wind waves excite primary and secondary microseisms, respectively, when they interact with the seabed. Periods of primary and secondary microseisms are directly proportional to the periods of sea wind waves, which are connected with the speed and time of action of the wind area and the depth of the basin over which the wind acts. The periods of microseisms are in the range of about 2 to 20 s. The periods of primary microseisms are equal to the periods of progressive wind waves. The periods of secondary microseisms are equal to the periods of standing sea waves, or are half of a period of progressive sea waves, because the variation in hydrostatic pressure in a standing sea wave changes twice in one period of a surface sea wave. The amplitudes of secondary microseisms can be either greater or smaller than the amplitudes of primary microseisms. If standing waves formed as a result of the interference of progressive waves with approximately equal amplitudes (for example, in the rear of a moving cyclone), then the amplitudes of primary microseisms will be smaller than the amplitudes of secondary microseisms. If standing waves formed as a result of the interference of progressive waves with very different amplitudes (oncoming and coast-reflected waves), then the amplitudes of primary microseisms will be greater than the amplitudes of secondary microseisms.

Paper [2] discusses the possibility of using microseismic signals, which result from the action of wind sea waves on the seabed, to obtain information about typhoons. Based on the main characteristics of the registered microseisms, by solving the inverse problem, we can determine (using the amplitude and period of the microseisms) the magnitude and period of the sea wind waves. In addition, using the dispersion equation when processing of the obtained experimental data make it possible to localize the area of generation of these sea waves [3], which, as a rule, coincides with the most energy-intensive part of the typhoon. Considering that the speed of microseism propagation is almost an order of magnitude greater than the speed of wind waves, this remote method of studying some parameters of typhoons and their manifestations is quite promising.

In [4], the relationship between microseisms and specific storms was studied. Great storms significantly increase microseismic energy [5–7], and their partial dissipation in the sea Earth’s crust leads to an increase in the temperature of the world’s oceans. In this regard, seismic noise variations recorded in the scope of decades were studied for their relationship with climate variability [8]. The works [9,10] established the relationship between microseisms and teleseismic body waves.

In addition to estimating the energy of storms generated by typhoons using microseismic data, everyone is interested in the possibility of tracking typhoon movements by its secondary manifestations, such as by variations in the main parameters of microseisms. One of the main parameters is the period of primary microseisms, which is equal to the period of progressive sea waves at the point of interaction of the latter with the seabed. An increase and decrease in the periods of microseisms, along with the mechanisms of developing waves and dispersion, are associated with the degree of change in the magnitude and direction of typhoon movement speed, i.e., the change in periods of microseisms is associated with the Doppler Effect [11]. It is this peculiarity that can be used in partial solution of the problem of finding a tropical cyclone’s direction. To solve this problem, we need to have the values of the investigated initial parameters at the time of tracking the typhoon’s movement.

In this work, we set goals for tracking the movements of typhoons (tropical cyclones) by sensing the directions of primary and secondary microseisms origination zones, and by sensing the directions of the “voice of the sea” origination zones [12]. “Voice of the sea” microseisms originate as a result of the “voice of the sea” microbaroms [13] on the upper layer of the Earth’s crust of the surf zone.

2. Two-Coordinate Laser Strainmeter

As a receiving system for primary and secondary microseisms and the “voice of the sea” microseisms, we used a two-coordinate laser strainmeter [14] consisting of an unequal-arm-type laser strainmeter with a measuring arm length of 52.5 m that was oriented at the angle of 18° clockwise relative to the “North–South” line and a laser strainmeter of unequal-arm-type from “West–East” with a measuring arm length of 17.5 m that was oriented at the angle of 92° relative to the 52.5 m laser strainmeter. All laser strainmeters are designed on the base on an unequal-arm-type Michelson interferometer, which uses frequency-stabilized helium-neon lasers as a light source with a frequency stability in 9–12 digits [15,16]. Figure 1 shows a general view of the underground beam guide (a) of the 52.5 m laser strainmeter with a central interference unit and a frequency-stabilized laser (b). Figure 2 shows a map scheme of the laser strainmeter’s location.

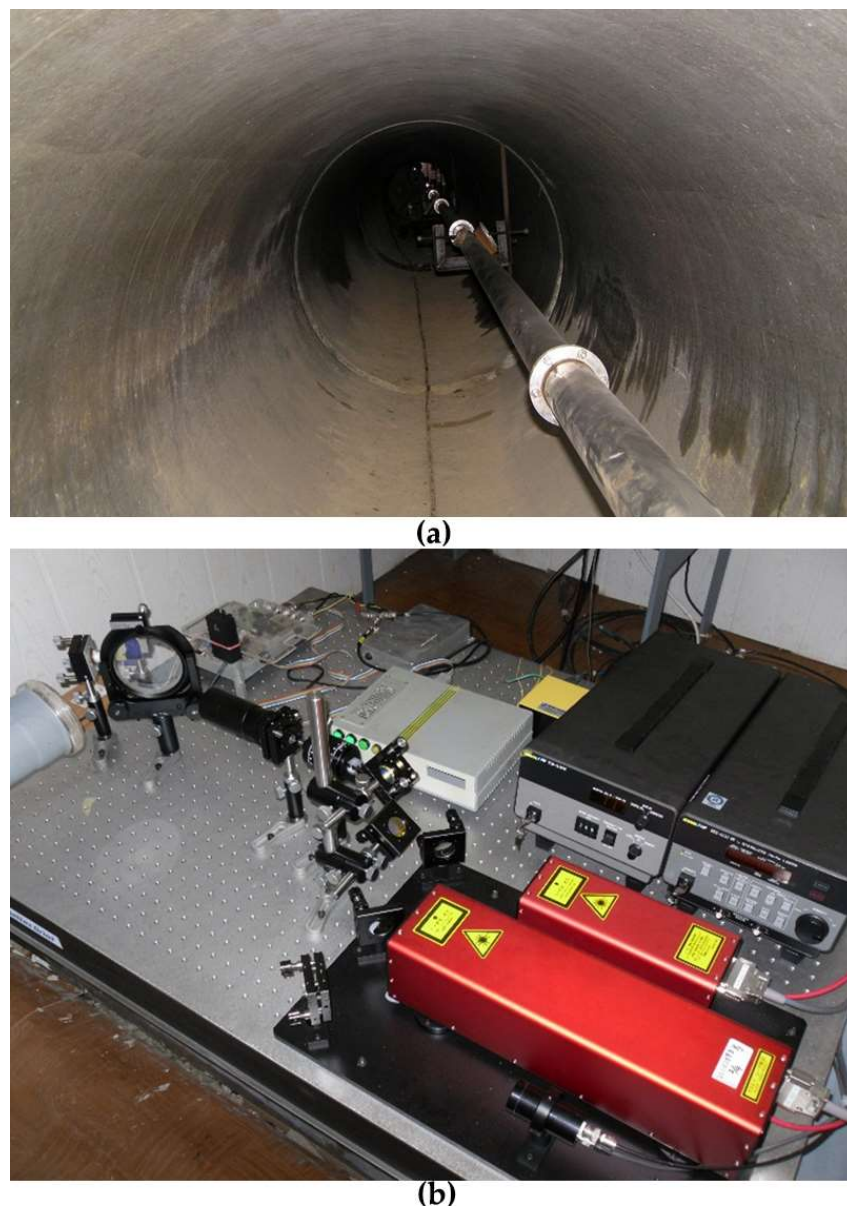


Figure 1. Underground beam guide of 52.5 m laser strainmeter of unequal-arm-type (a) and central interference unit (b).



Figure 2. Scheme of arrangement of laser strainmeters. 1—laser strainmeter with measuring arm length of 52.5 m, 2—laser strainmeter with measuring arm length of 17.5 m, 3—laboratory building.

The used interferometry methods, which consist of tracking the changes in light wave phases in the Michelson interferometer with high accuracy (widely known in the sphere of optics since the 19th century), make it possible to measure the displacements of the laser strainmeters abutments relative to each other, with an accuracy of 10 pm, which, when taking into account the lengths of the laser strainmeters' arms, is equal to the deformation of 0.19×10^{-12} (for the strainmeter with the arm length of 52.5 m) and 0.57×10^{-12} (for the strainmeter with arm of 17.5 m). The principle of operation of this method in our interferometer is similar to the principle of operation of the interference method, which was applied in the construction of the LIGO interferometers [17]. The laser strainmeters, together with other recording equipment, are located at Shultz Cape in the Peter the Great Bay, the Sea of Japan. At all devices, continuous measurements of various geosphere parameters variations were carried out in the frequency range from 0 Hz (conditionally) to several kilohertz. The obtained experimental data after pre-processing (filtration and decimation) entered the laboratory room (label 3 in Figure 2) where it was recorded on a hard drive. Subsequently, this data was transported to Vladivostok and placed in the previously created experimental database for final system processing, depending on the set of scientific tasks.

3. Processing and Analysis of the Obtained Experimental Data

When processing the experimental data of the laser strainmeters of the microseismic range, we can, first of all, estimate the power of the primary sources of wind waves and, when taking into account the dispersion equation and application of the technique

described in [3], we can accurately calculate the distance from the place of wind sea waves generation, which, during a typhoon movement, is associated with the place of the highest wind speed in the typhoon, i.e., with the place of greatest typhoon energy. This is an extremely important result in predicting the probable effects of typhoons on specific regions of the globe.

In the initial part of this section of the paper, we evaluate the possibility of using the parameters of primary microseisms to solve the problem of finding typhoon direction. Let us consider this issue when processing and analysing data from the two-coordinate laser strainmeter recording Typhoon Hagupit's passage over the Sea of Japan. Category 1 Typhoon Hagupit formed on 31 July 2020 in the Philippine Sea of the Pacific Ocean. It was the fourth named storm and the second typhoon of the 2020 season. The intensity of the storm peaked when pressure in the centre of the cyclone dropped to 975 Pa. The cyclone passed along the east coast of China, as a result of which it began to weaken and reduced to a tropical storm on 3 August. When the cyclone entered the Yellow Sea, its rating dropped to a tropical depression, and it then passed over into the category of an extratropical cyclone. In this status, the cyclone entered the Sea of Japan on 6 August. At the same time, despite the extratropical transition, meteorological agencies continued to track Hagupit as a tropical storm until 12 August due to the preservation of the vortex structure and energy balance from the heating water surface of the middle latitudes. Figure 3 shows the movement of Typhoon Hagupit.

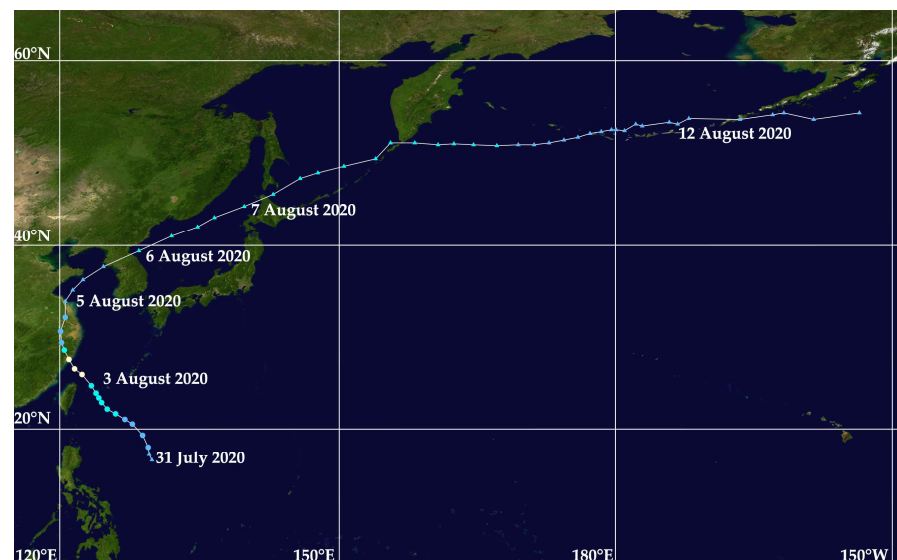


Figure 3. Trajectory of Typhoon Hagupit in the Pacific Ocean zone.

This typhoon, upon its impact on the Sea of Japan, excited surface sea waves in it, which subsequently caused primary and secondary microseisms. The maximum period of primary microseisms, which were identified during the processing of laser strainmeter data, was about 10.6 s, and the maximum period of secondary microseisms was about 5.3 s. When processing the entire array of data from the laser strainmeters during the typhoon passage across the Sea of Japan in the period from 5 August 2020 to 7 August 2020, the best fragment of the record was selected for further analysis, in which primary and secondary microseisms were clearly distinguished and where other powerful spectral components of adjacent frequency ranges had the least effect on the microseisms. This selected time segment began at 03:30 p.m. on 6 August and ended at 1:30 a.m. on 7 August. Figure 4a shows the spectrogram of the 52.5 m laser strainmeter record fragment, which traced primary microseisms (about 10 s) and secondary microseisms (about 5 s). The record fragment considered in Figure 4 includes the above-mentioned time. The same figure (b) shows the spectrogram of the same time fragment of the 17.5 m laser strainmeter, on which secondary microseisms are clearly pronounced and primary microseisms are faintly visible. Their amplitudes are

slightly above the background. They are practically invisible in this figure, but they stand out quite clearly during spectral processing of the individual fragments of the 17.5 m laser strainmeter record. Thus, Figure 5 shows the spectra of the microseismic range of the synchronous fragments of the 52.5 m and 17.5 m laser strainmeters records. As we can see from the above spectra, the amplitude of the primary microseisms in the 52.5 m laser strainmeter record was more than an order of magnitude higher than the amplitude of the primary microseisms isolated from the 17.5 m laser strainmeter record. Moreover, the magnitudes of neighbouring components near the primary microseisms of the 17.5 m laser strainmeter were slightly smaller than the main spectral maximum of the primary microseisms. The maximum, which was responsible for the secondary microseisms of the 17.5 m laser strainmeter, was much higher than the neighbouring spectral maxima. This affected the visual picture shown in Figure 4.

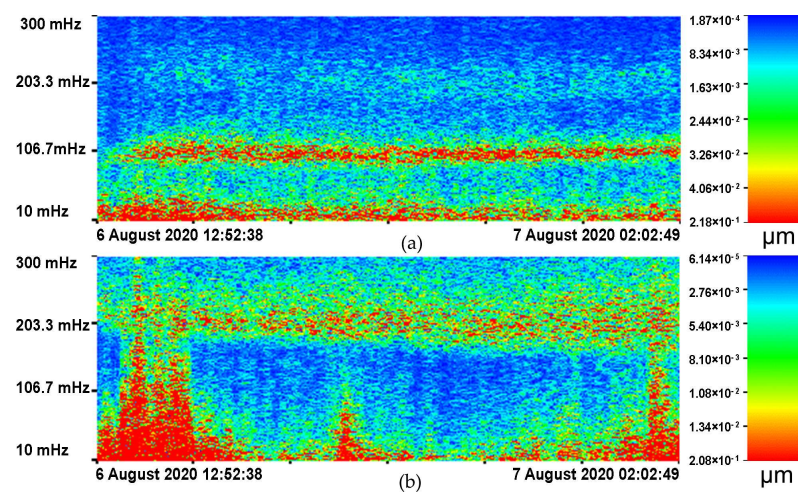


Figure 4. Spectrograms of fragments of the records measured by 52.5 m laser strainmeter (a) and 17.5 m laser strainmeter (b).

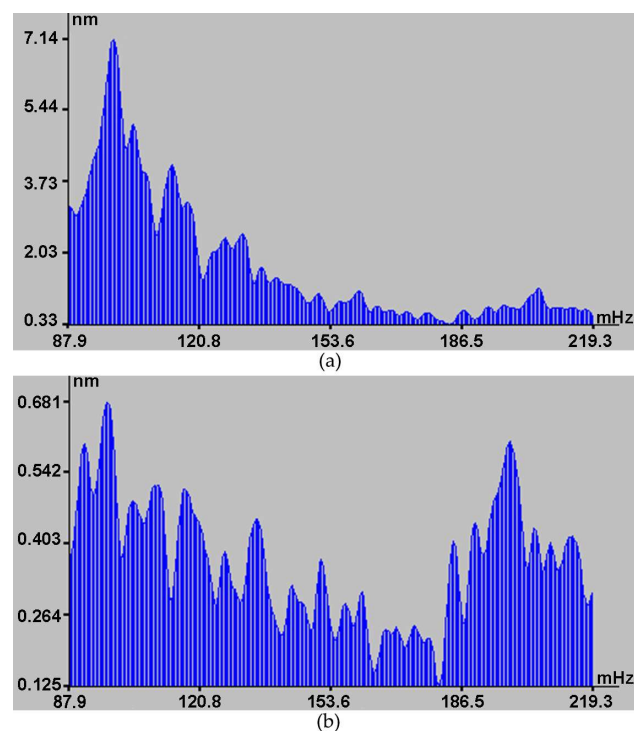


Figure 5. Spectra of synchronous fragments of 52.5 m laser strainmeter (a) and 17.5 m laser strainmeter (b) records.

In the time interval under consideration, the typhoon was moving as is shown in Figures 6 and 7.

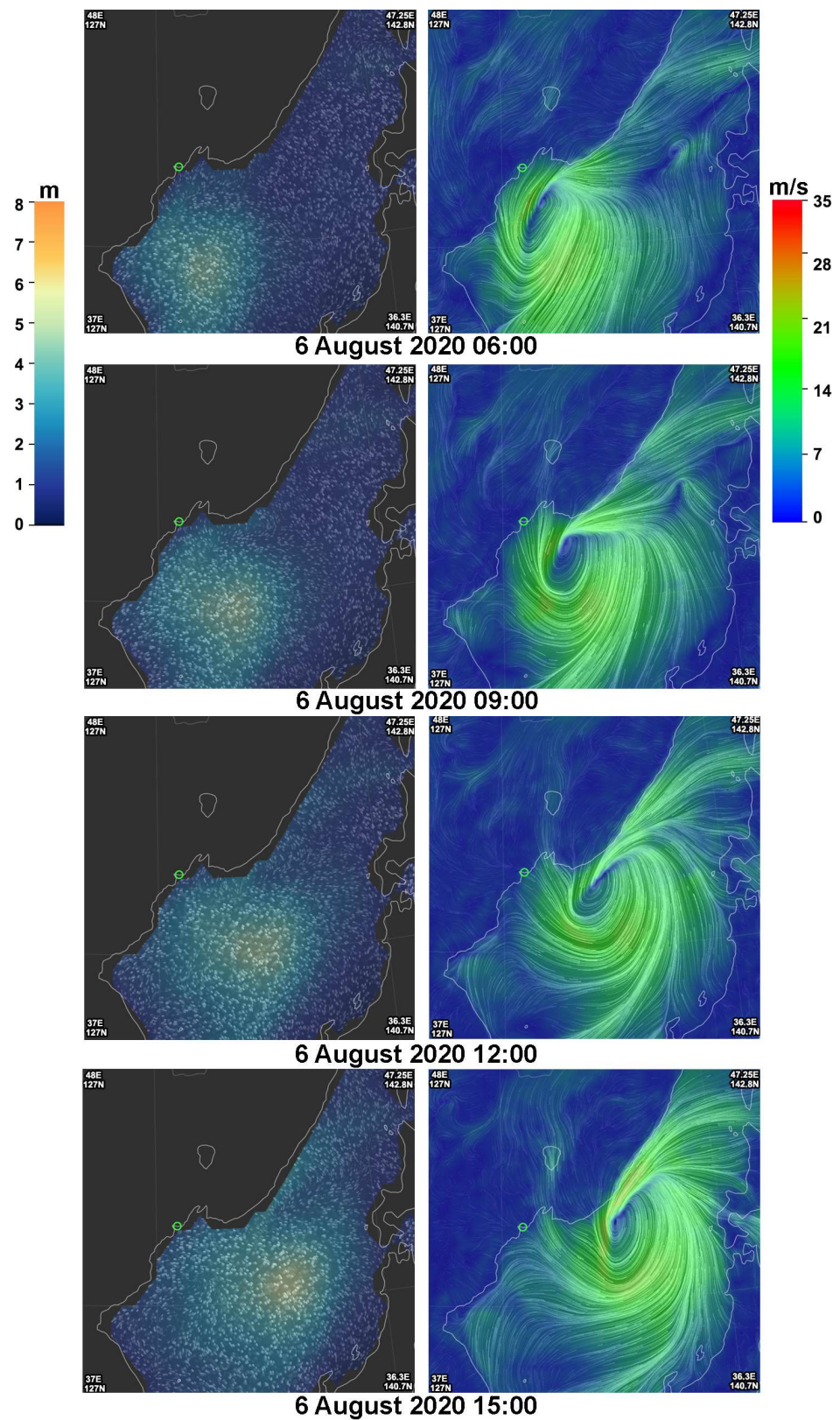


Figure 6. Wind waves and wind speeds as the typhoon moved on 6 August 2020 (UTC).

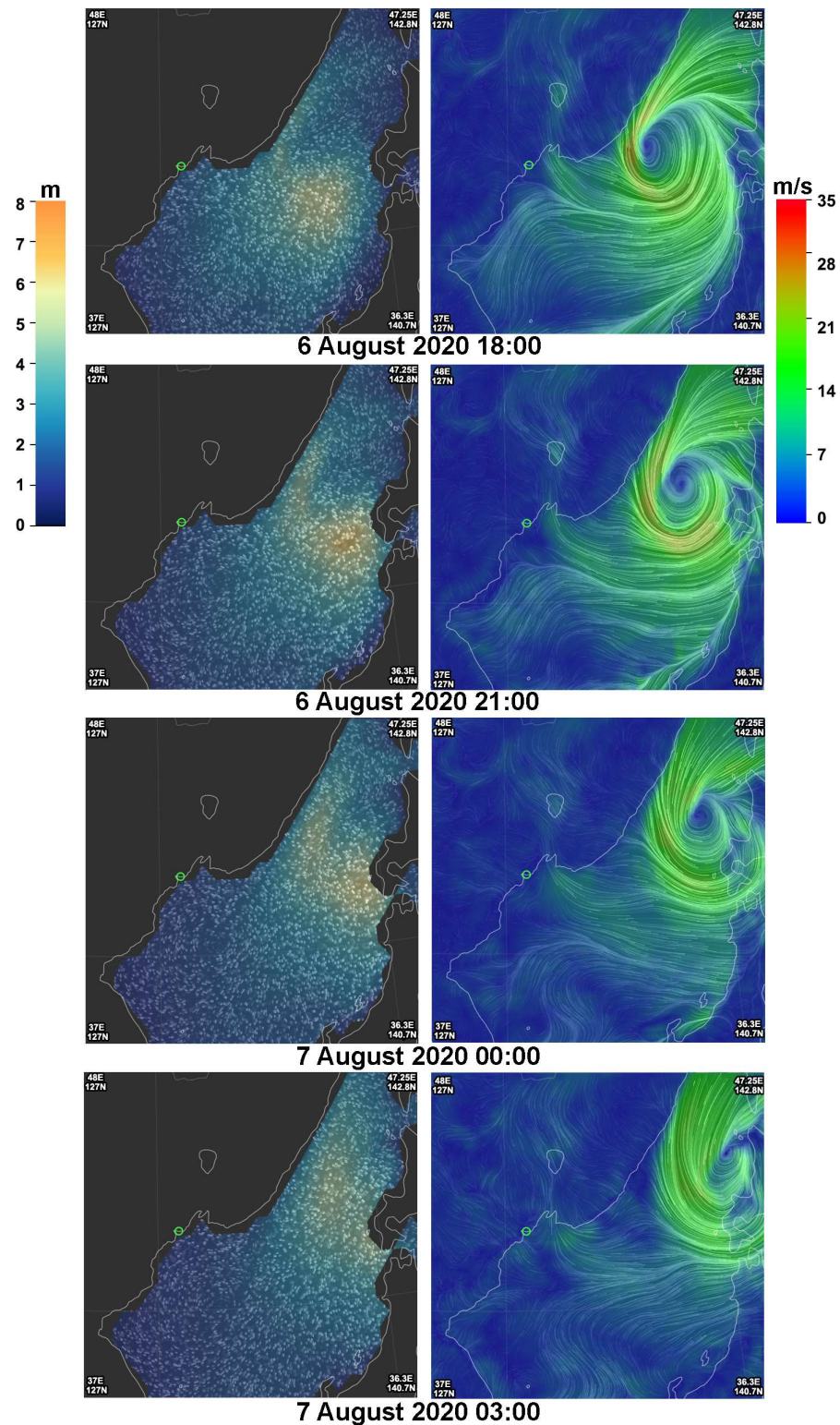


Figure 7. Wind waves and wind speeds as the typhoon moved on 6 August 2020–7 August 2020 (UTC).

During their propagation, sea progressive wind waves, while interacting with the seabed at depths of about and less than a half of a wind wave length, generate primary microseisms in the sea Earth's crust, which propagate over great distances [2]. These microseisms relate to surface waves of the Rayleigh type, in which particle oscillations occur around elliptical orbits along the path of a microseismic wave, i.e., they have longitudinal

polarization. We can register these microseisms with seismoacoustic receiving systems, such as laser strainmeters, and use them to try to determine the places of their generation. But the difficulty of fulfilling these intentions is in the fact that, due to refraction, an incident wind wave on the shelf will always move towards the coast, and, wherever a typhoon is in the sea, we cannot determine its direction. We can only estimate the direction of the place of generation of the registered primary microseisms, which are caused by wind waves generated by a typhoon/cyclone. These conclusions are also confirmed by the results given in Table 1. This table shows the bearing to the source of primary microseisms, which were calculated from the data of the 17.5 m and 52.5 m laser strainmeters relative to the axis of the 52.5 m laser strainmeter. Sensing the direction of the zone of primary microseisms generation was carried out using the data from the 52.5 m and 17.5 m laser strainmeters. For each time interval, which are presented in the first column of Table 1, we determined the amplitudes of the primary microseisms measured by the 52.5 m and 17.5 m laser strainmeters. Based on the correlation of the measuring arms of the 52.5 m and 17.5 m laser strainmeters with the equal external load on the laser strainmeters, the correlation of the displacement values of the laser strainmeters to each other should be $52.5:17.5 = 3.0$. This condition was met when the laser strainmeters were installed on the medium with absolutely identical elastic characteristics. But in situ conditions could not be achieved. However, this correlation could be estimated with identical impacts of atmosphere pressure variations on the Earth's crust areas, which were occupied by these laser strainmeters. We carried out this work and, as a result, established that, with identical external force action on the Earth's crust at the strainmeters' locations, this correlation equaled not 3.0, but 2.8. We used this correlation for sensing the direction of the sources of various signals—hydroacoustic, seismoacoustic, geophysical, etc. In our case, finding the direction was determined by the tangent $tg\alpha = 2.8 \times a_{17.5}/a_{52.5}$ where α is the angle between the direction to the signals' source and axis of the 52.5 m laser strainmeter, $a_{17.5}$ is the amplitude of the spectral component of the 17.5 m laser strainmeter, and $a_{52.5}$ is the amplitude of the spectral component of the 52.5 m laser strainmeter. We most certainly took into account that primary microseisms relate to the Rayleigh-type surface waves that have longitudinal polarization. Secondary microseisms relate to Love waves that have transverse polarization. We took this into consideration when calculating the direction of the secondary microseisms' generation zones (the last column of Table 1).

As we can see from Table 1, despite the typhoon movement relative to the location of the laser strainmeters, the bearing given in Table 1 accounts for errors in determining wave amplitudes according to the data of the laser strainmeters and non-stationarity of the processed series, which practically did not change. Where is the place of generation of primary and secondary microseisms, which does not depend on the typhoon location?

To answer this question, let us analyse some of the data presented in Table 2. The main data presented in Table 2 is taken from [18]. The columns of the table contain the following information: (1) Date of information retrieval when the typhoon was in the area in accordance with Figure 6. (2) Parameters of the wind waves in the epicentre of the greatest waves (maximum wave period and wave height). (3) Parameters of the wind waves near the Gamow Peninsula and Furugelm Island (maximum wave period and wave height). (4) Distance from the epicentre of the maximum wind waves to the location of the laser strainmeters. (5) Speed of the wind wave, based on the condition that the wind wave propagated through deep water, which was calculated using the formula $C^2 = g\lambda/2\pi$, where C is speed, λ is wavelength, and T is period (or at $C = \lambda/T$, $C \approx gT/2\pi$ [19]). 6. The propagation time of this wave from the epicentre of the greatest wave to the measuring site location. If we compare the data given in the third column of Table 2 and our data given in the second column of Table 1, we can note that they coincide quite accurately. We took the data presented in the second and third columns from wave charts [18], which were taken every three hours. The periods and amplitudes of the waves near the shore were taken at approximate locations near Gamow Cape and Furugelm Island. In Table 3, we present data on the waves near the shore, which were taken from Table 2, and data from Table 1

at approximately the same time. This suggests that primary microseisms, recorded by the laser strainmeter, indeed formed in the shelf area and near the coast: this zone includes the Gamow Peninsula and Furugelm Island. The direction of the place of the greatest generation relative to the axis of the 52.5 m laser strainmeter was, on the average, 27.4° . In view of the fact that the axis of the 52.5 m laser strainmeter was at the angle of 18° to the North–South line, we can state that, relative to the North–South line, the place of primary microseisms generation was located along the direction of the straight line at the angle of 45.4° relative to the North–South line. This place of generation of the primary microseisms can be found from the diagram, which is shown in Figure 8. Considering that the place of primary microseisms generation was located on the shelf near the surf zone, according to Figure 8, we could find this zone. The blue line is the direction of the generation zone of the primary microseisms. The brown line is the direction of the generation zone of the secondary microseisms. This zone was located at the intersection of the abovementioned direction with the coast. There may be 2–3 of such zones, but, most likely, this zone was located near the Kyongsong-man Bay and was bounded by the Orang-dan Cape from the south and the Komalsan-dan Cape from the north. Probably, a zone of primary microseisms with maximum amplitude generation was located at one of these capes.

Table 1. Direction of areas of primary and secondary microseisms generation.

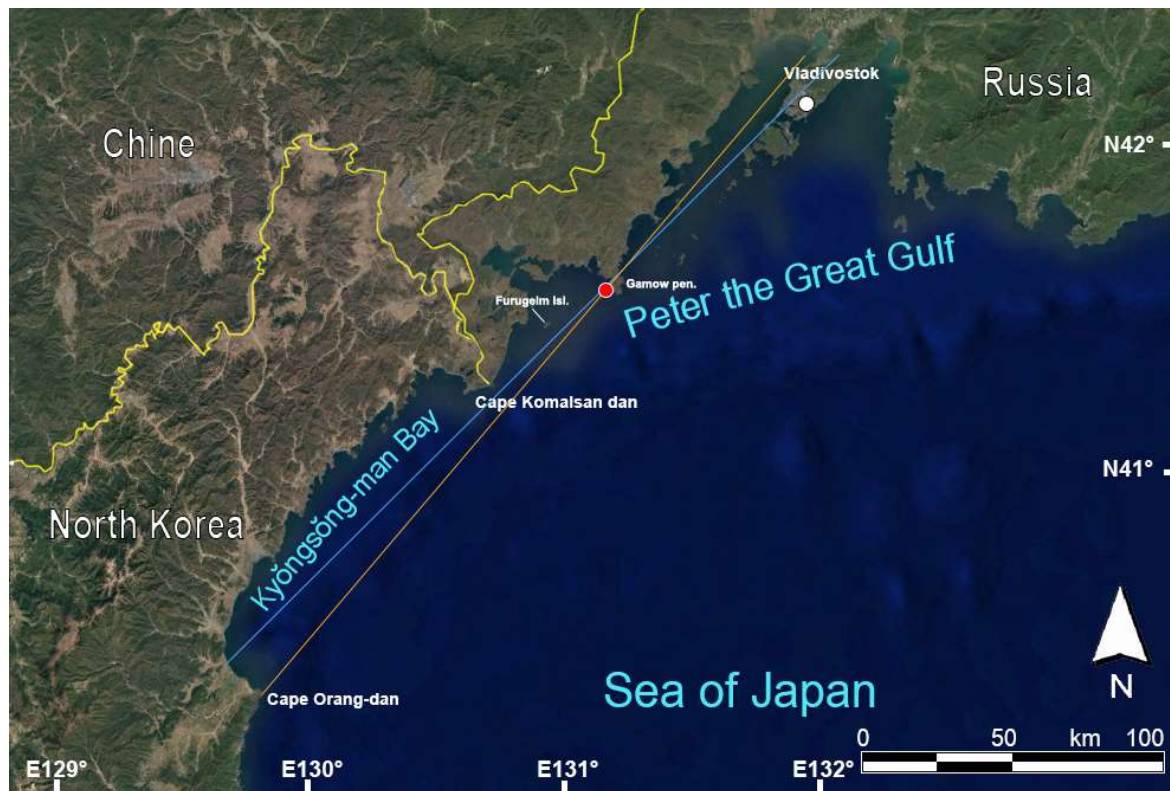
Date, Time	Primary Microseisms. Longitudinal Wave		Angle of Incidence on the Axis of 52.5 m Laser Strainmeter	Secondary Microseisms. Transverse Wave		Angle of Incidence on the Axis of 52.5 m Laser Strainmeter
	52.5 m Laser Strainmeter. Period, s.	17.5 m Laser Strainmeter. Period, s.		52.5 m Laser Strainmeter. Period, s.	17.5 m Laser Strainmeter. Period, s.	
August 6						
15:29:06	9.9	9.6	32.3	4.1	4.8	27.9
15:53:45	9.9	9.9	27.1	4.7	4.7	25.2
16:29:51	10.1	10.2	28.4	4.4	5.0	20.4
17:05:58	9.5	9.3	28.9	4.8	4.6	24.3
17:42:04				4.7	5.2	21.8
18:18:11	9.8	9.8	32.3	4.8	5.1	18.7
18:54:18	9.9	10.1	36.5	5.2	5.2	18.4
19:30:25	9.8	9.9	33.4	4.8	5.3	24.7
20:06:31	9.5	9.6	25.0	5.1	5.4	20.9
20:42:38	9.4	10.1	23.9	4.8	4.8	19.1
21:40:18	9.4	9.3	28.0	5.3	5.3	16.8
21:54:51	9.9	10.2	21.4	5.0	5.0	21.6
22:30:58	9.4	9.2	20.5	4.8	5.4	18.4
23:07:05	9.4	9.7	29.2	5.2	5.2	17.3
23:43:11	9.4	9.5	24.8	4.8	5.2	18.5
August 7						
00:19:18	9.0	9.5	22.5	4.6	4.9	20.5
00:55:25	9.5	9.8	27.6	4.6	5.3	23.6
01:31:31	9.3	9.3	24.6	4.6	5.1	22.9
Average bearing			27.4			22.4
Variance			18.5			10.5
Standard deviation			4.3			3.2

Table 2. Information on wind waves in the epicentre of the Sea of Japan waves and near the Gamow Peninsula and Furugelm Island [18].

Date	Waves in the Epicentre	Waves Near the Coast	Distance, km	Speed, m/s	Propagation Time
06:00 06.08.2020	9.6 s/5.15 m	5 s/1.68 m	320	15.0	5 h 55 min 33 s
09:00 06.08.2020	10.1 s/5.42 m	5.5 s/1.85 m	280	15.8	4 h 55 min 22 s
12:00 06.08.2020	10.7 s/5.56 m	7.6 s/1.92 m	310	16.7	5 h 09 min 23 s
15:00 06.08.2020	11.0 s/6.52 m	9.6 s/2.20 m	380	17.2	6 h 08 min 13 s
18:00 06.08.2020	11.4 s/6.60 m	9.5 s/2.07 m	450	17.8	7 h 01 min 21 s
21:00 06.08.2020	11.8 s/7.67 m	9.3 s/1.81 m	550	18.4	8 h 18 min 11 s
00:00 07.08.2020	12.3 s/7.25 m	9.0 s/1.46 m	600	19.2	8 h 40 min 50 s
03:00 07.08.2020	10.0 s/5.44 m	8.6 s/1.24 m	630 (but to the north 200 km)	15.6	11 h 13 min 5 s
06:00 07.08.2020	10.0 s/5.16 m	8.3 s/1.07 m		15.6	

Table 3. Data on periods of swell waves and periods of primary microseisms.

Table	Time	Period, s						
Table 2	15:00	9.6 c	18:00	9.5 c	21:00	9.3 c	00:00	9.0 c
Table 1	15:29	9.9–9.6 c	18:18	9.8 c	21:40	9.4–9.3 c	00:19	9.0–9.5

**Figure 8.** Diagram of direction of microseisms' generation zones. Red circle is the location of the laser strainmeters.

Let us pay some attention to the data, given in Table 2, which we received from the site <https://earth.nullschool.net> (accessed on 10 September 2022) [18]. It is somewhat puzzling that no swell was registered near the coast, which came from the zone of action of the typhoon vortex with long periods—12 s. If it was registered in the epicentre of the greatest wind waves, then it must come to the coast. When leaving the zone of a storm of wind action, the wind waves, having transformed into swell waves, slightly change with the loss of shorter-period disturbances, but long waves should persist and reach the coast without much transformation of the period. This discrepancy is very interesting and requires further study.

Now let us pay attention to the range of the “voice of the sea” microseisms, which are generated by passing typhoons and were recorded by the laser strainmeters and a broadband seismograph [12]. Let us analyse the data of the laser strainmeters in this frequency range during passage of the above typhoon (Hagupit), and also two typhoons from 2015, Chan-Hom and Matmo, whose tracks are shown in Figure 9.

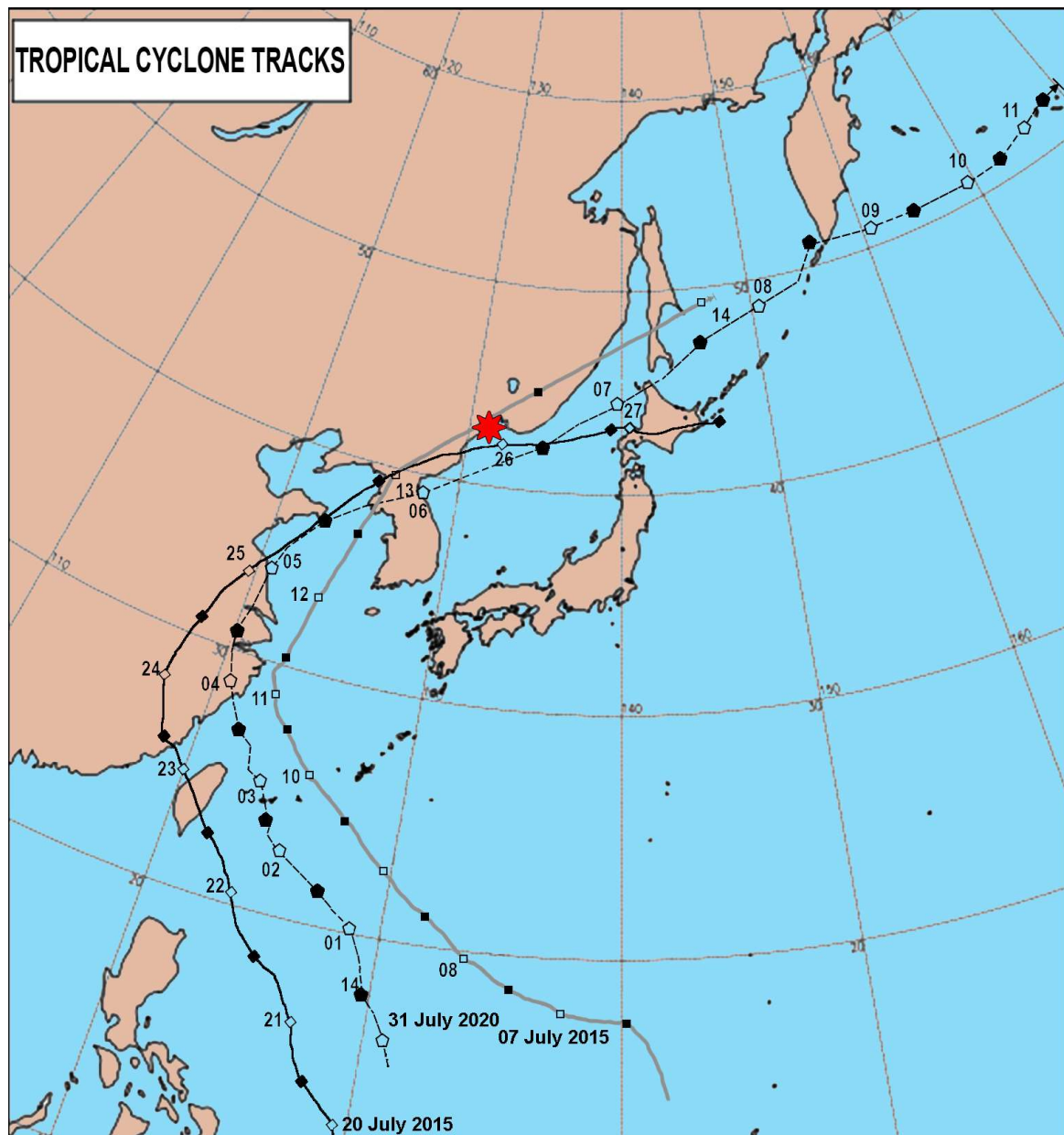


Figure 9. Integrated map of typhoons tracks, where: Red asterisk—location of the laser strainmeters; ■—Typhoon Chan-Hom; ◆—Typhoon Matmo; ●—Typhoon Hagupit.

Typhoon Hagupit passed through the Sea of Japan along the Primorsky Territory on 6 and 7 August 2020; its centre entered the Sea of Japan from the Korean Peninsula to the East Korea Bay. Before this entry, the lateral tail of the vortex stretched from the Korea Strait to the point of exit to the Sea of Japan. After the typhoon entered the Sea of Japan, a powerful wind impact appeared in the opposite direction. The typhoon moved to the central part of the Sea of Japan in less than 6 h without creating significant waves there. According to the data of the two-coordinate laser strainmeter, we found that the “voice of the sea” microseisms were observed for less than a day. The places of their generation are shown in Figure 10, wherein the area of generation of the “voice of the sea” microseisms moved over time along the eastern coast of the Korean Peninsula.

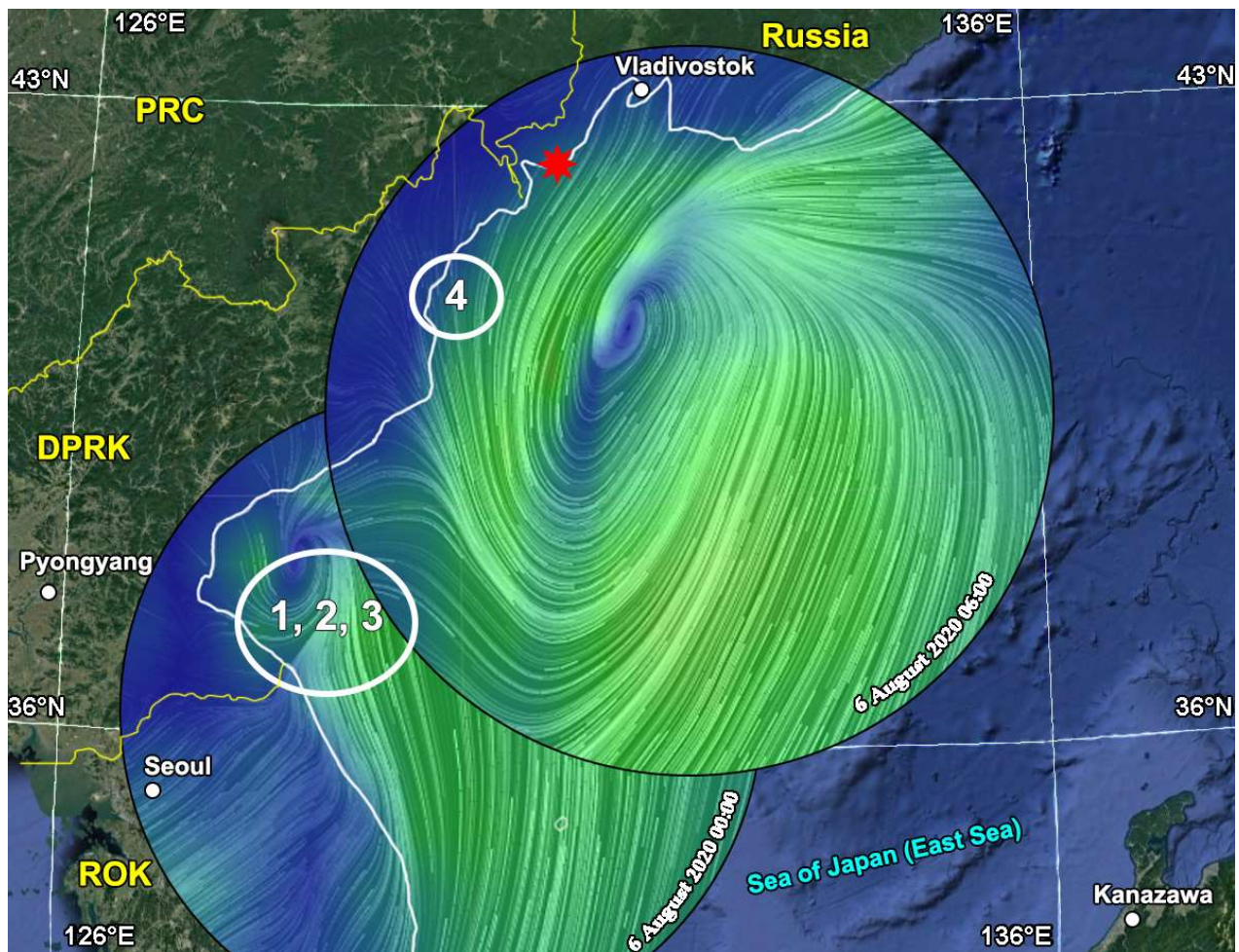


Figure 10. Areas of the “voice of the sea” microseisms generation; 1–4—successive (over time) areas of the “voice of the sea” microseisms generation. Red asterisk indicates the location of the two-coordinate laser strainmeter.

Typhoon Matmo spent most of its energy over the Southeast Asian region as it entered the Sea of Japan, but still had enough energy to generate wind waves in the Sea of Japan. It gained strength again while crossing the Sea of Japan. Approaching the islands of Japan, the typhoon took an orderly form near the Japanese islands and lingered off the western coast of the Japanese island of Hokkaido. During this time, in the interval of 26 July and 27 July 2014, the microseismic signal of the “voice of the sea” was observed up to the moment when the influence of the typhoon on the Sea of Japan ceased. According to the data of the two-coordinate laser strainmeter, we determined the generation areas of the “voice of the sea” microseisms; their sequence of movement is shown in Figure 11.

The third typhoon, Chan-Hom, had a significant impact on the Sea of Japan on 13 and 14 July 2015. The appearance of the “voice of the sea” microseisms began after the centre of the typhoon vortex crossed the coastline with the beginning of a strong wind impact from the rear of the cyclone onto the Peter the Great Bay area. According to the data of the two-coordinate laser strainmeter, we determined the areas of the “voice of the sea” microseisms generation; the sequence of their movements is shown in Figure 12.

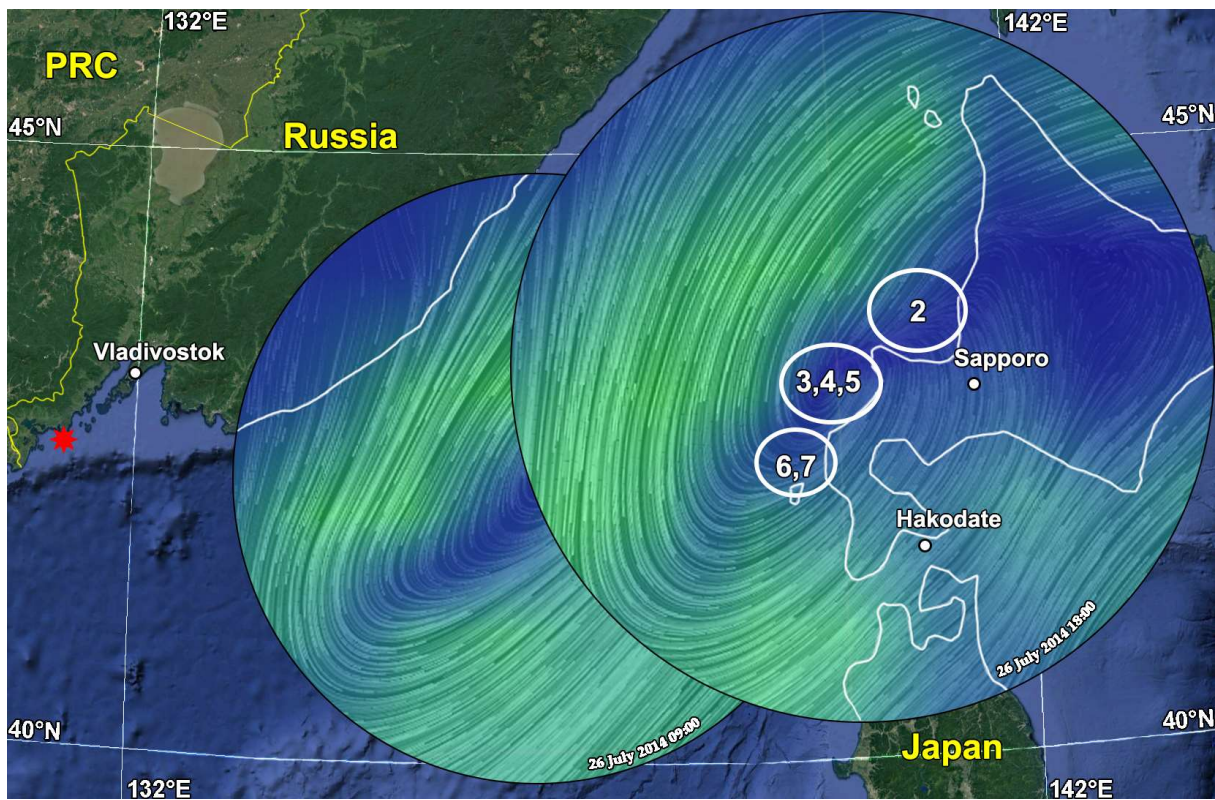


Figure 11. Areas of the “voice of the sea” microseisms generation; 2–7—successive (over time) areas of the “voice of the sea” microseisms generation. Red asterisk indicates the location of the two-coordinate laser strainmeter.

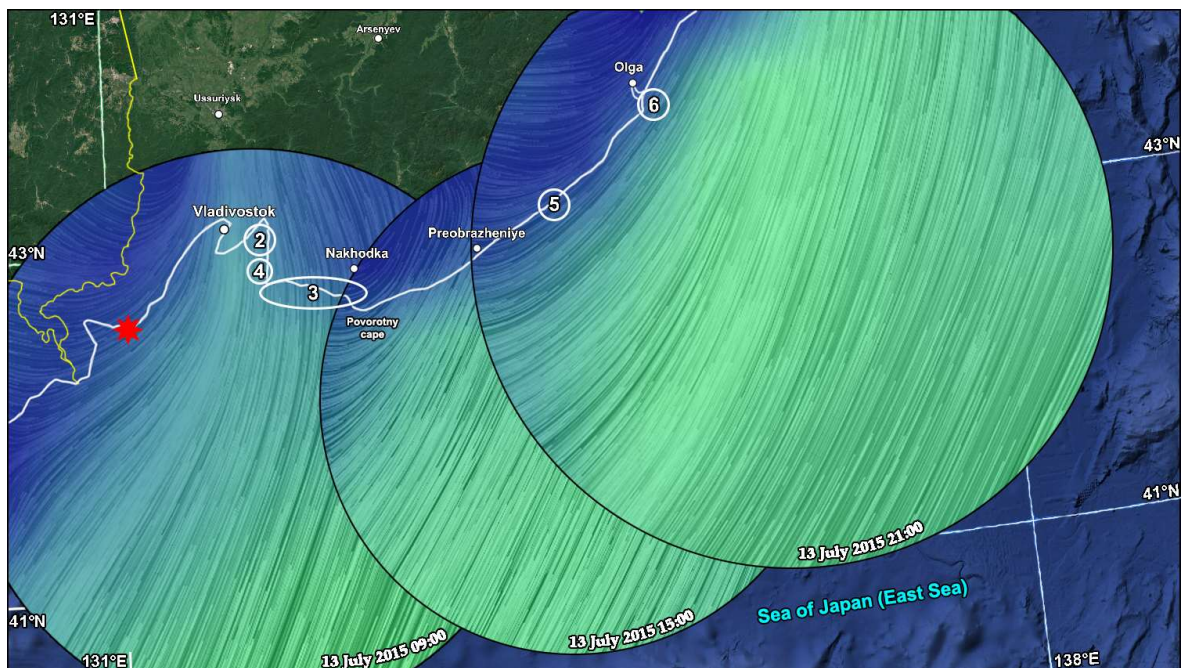


Figure 12. Areas of the “voice of the sea” microseisms generation; 2–6—successive (over time) areas of the “voice of the sea” microseisms generation. Red asterisk indicates the location of the two-coordinate laser strainmeter.

Based on Figures 10–12 and the analysis of satellite data, it follows that the typhoon sequentially moved along the coast of the Korean Peninsula (Figure 10), Hokkaido Island (Figure 11), and the Primorsky Territory (Figure 12), where it generated “voice of the sea” sound waves during its propagation, which, in turn, generated the “voice of the sea” microseisms. Thus, by determining the direction to the formation zones of the “voice of the sea” microseisms, we can find the direction of the zones of the highest energy capacity of typhoons.

4. Discussion

Let us now turn to finding the direction of the secondary microseisms’ zone generations. We will describe the mechanism of secondary microseisms formation in accordance with the classical concept. Secondary microseisms are formed as a result of variable hydrosphere pressure, which is exerted on the seabed by standing sea waves. Standing sea waves are formed as a result of the nonlinear interaction of progressive sea waves: (1) in the rear of a moving cyclone, (2) near the coastal zone with nonlinear interaction of oncoming and coast-reflected progressive waves, (3) near the rear (relative to the open sea) part of the islands with nonlinear interaction of progressive wind waves, which, due to refraction, circle the island from two sides. The period of standing waves is twice as short as the period of progressive waves. In accordance with this, period of secondary microseisms is two times shorter than the period of the corresponding primary microseisms. Secondary microseisms are related to Love waves and have transverse polarization. We determined the periods of secondary microseisms and their amplitudes basing on the experimental data of the laser strainmeters. The values of the periods of secondary microseisms are presented in Table 1. According to the experimental data, obtained from the 17.5 m and 52.5 m laser strainmeters, and taking into account the polarization of secondary microseisms, we determined the direction to the supposed place of their formation, listed in Table 1. It was at the angle of 22.4° clockwise relative to the axis of the 52.5 m laser strainmeter or 40.4° clockwise relative to the North–South line. Considering a slight discrepancy in the directions of the place of formation of the primary and secondary microseisms, we can state that the places of their generation were approximately in the same zone.

Now let us discuss the issue that is undoubtedly interesting to everyone. Sea waves, which are generated by a specific cyclone, propagate from the place of generation in various directions. As they interact with the seabed, they generate microseisms everywhere. Why did we choose one general direction of the zone of microseisms occurrence? Is it correct? Everything seems to be clear with secondary microseisms. As we remember, they originate as a result of the impact of standing sea waves on the seabed. The formation of standing sea waves in the rear of a moving cyclone is an extremely rare case. The speed of a cyclone has to be significantly greater than the swell waves, generated by it earlier, in order for the cyclone to overtake these wind waves (or swell waves) and excite other wind waves, which, when propagating previously formed wind waves and interacting with them, form standing sea waves. This was the rarest event that we did not find in the literature descriptions of any experiments. Regarding the reflection from the coast, as a rule, the wave reflected from the vertical coast has an amplitude of no more than 5% of the incident wave. When the oncoming and reflected waves interact, a standing wave of minor amplitude originates (square root of the product of the amplitudes). The third case stands apart—the formation of a standing wave as a result of the nonlinear interaction of progressive wind waves that have circled an island from two sides and, due to refraction, are moving towards each other. With such a mechanism, the amplitude of these waves will be comparable to the amplitudes of the incident waves. Moreover, the secondary microseisms, generated with this mechanism, will have the largest amplitude, which will be much greater than the amplitudes of the secondary microseisms formed with the second mechanism. The islands in our general direction of the microseism generation zone allowed us to assert that the third mechanism was working. When generating, primary microseisms will have higher amplitudes where the amplitude of swell waves is higher. In addition, we need to take into

account the bathymetry and change in the sea depth when a wave propagates along the shelf. The magnitude of microseisms will be greater where there is an abrupt change in depth, especially in the surf zone. However, if we look at the top curve in Figure 5, we can note that the spectrum of primary microseisms is stretched along the abscissa axis and has several peaks. This also indicates that the laser strainmeter registered primary microseisms from not one, but from several zones, but the largest maximum among the primary microseisms corresponded to the calculated direction.

5. Conclusions

By processing the experimental data of the two-coordinate laser strainmeter in the microseismic range and in the “voice of the sea” microseismic range, we studied the possibilities of using the processing results to obtain information about the main energy characteristics of typhoons and the possibilities of remote direction-finding of typhoons or their most energy-intensive areas. We have established that primary and secondary microseisms can be used to estimate the main parameters of wind waves (period and amplitude of sea waves) generated by typhoons. Also, by using dispersion equations, the Doppler equation, and the technique described in [11], we solved the inverse problem of determining the distance from the place of primary microseisms generation to the place of wind waves generation.

It is impossible to find the direction of the place of wind waves generation by primary and secondary microseisms, which were registered by the two-coordinate laser strainmeter, but it is possible to find the direction of the areas of primary and secondary microseisms generation.

Based on an account of the mechanism of the “voice of the sea” atmospheric infrasound disturbances and the “voice of the sea” microseisms formation as well as the data from the two-coordinate laser strainmeter, it is possible to find the direction of areas of the “voice of the sea” microseisms generation, which coincided with the zones of maximum energy of typhoons and the movement of the “voice of the sea” microseisms formation zones to find the direction of the locations of typhoons in the “sea-continent” transition zone.

Author Contributions: G.D.—problem statement, discussion, and writing of the article. S.D.—data processing, discussion, and writing of the article. V.C.—data curation, visualization. A.D.—data curation, software. A.M.—formal analysis, supervision. All authors have read and agreed to the published version of the manuscript.

Funding: The work was supported in part by the State Assignment under Grant AAAA-20-120021990003-3 “Investigation of fundamental bases of generation, development, transformation and interaction of hydroacoustic, hydrophysical and geophysical fields of the World Ocean” (instrumentation setup, physical measurements) and part of the Laboratory of Nonlinear Hydrophysics and Natural Hazards of V.I. Il’ichev Pacific Oceanological Institute, Far Eastern Branch Russian Academy of Sciences, the Ministry of Science and Education of Russia, project agreement No 075–15-2022–1127 from 1 July 2022 (processing and interpretation of data obtained).

Data Availability Statement: 3rd Party Data. Restrictions apply to the availability of these data.

Acknowledgments: We would like to express our deep gratitude to all employees of the Physics of Geospheres laboratory.

Conflicts of Interest: The authors declare no conflict of interest.

References

1. Hasselmann, K. A statistical analysis of the generation of microseisms. *Rev. Geophys* **1963**, *1*, 177–209. [[CrossRef](#)]
2. Ebeling, C.W.; Stein, S. Seismological Identification and Characterization of a Large Hurricane. *Bull. Seismol. Soc. Am.* **2011**, *101*, 399–403. [[CrossRef](#)]
3. Dolgikh, G.I.; Dolgikh, S.G.; Budrin, S.S. Fluctuations of the sea level, caused by gravitational and infra-gravitational sea waves. *J. Mar. Sci. Eng.* **2020**, *8*, 796. [[CrossRef](#)]
4. Gerstoft, P.; Fehler, M.; Sabra, K. When Katrina hit California. *Geophys. Res. Lett.* **2006**, *33*, L17308. [[CrossRef](#)]
5. Astiz, L.; Creager, K. Geographic and seasonal variations of microseismic noise. *Eos Trans.* **1994**, *75*, 419.

6. Bromirski, P.; Flick, R.; Graham, N. Ocean wave height determined from inland seismometer data: Implications for investigating wave climate changes in the NE Pacific. *J. Geophys. Res.* **1999**, *104*, 20753–20766. [[CrossRef](#)]
7. Grevemeyer, I.; Herber, R.; Essen, H.H. Microseismological evidence for a changing wave climate in the northeast Atlantic Ocean. *Nature* **2000**, *408*, 349–352. [[CrossRef](#)] [[PubMed](#)]
8. Aster, R.; McNamara, D.; Bromirski, P. Multidecadal climate-induced variability in microseisms. *Seismol. Res. Lett.* **2008**, *79*, 194–202. [[CrossRef](#)]
9. Landès, M.; Hubans, F.; Shapiro, N.; Paul, A.; Campillo, M. Origin of deep ocean microseisms by using teleseismic body waves. *J. Geophys. Res.* **2010**, *115*, B05302. [[CrossRef](#)]
10. Zhang, J.; Gerstoft, P.; Shearer, P. Resolving P-wave travel-time anomalies using seismic array observations of oceanic storms. *Earth Planet. Sci. Lett.* **2010**, *292*, 419–427. [[CrossRef](#)]
11. Dolgikh, G.I.; Mukomel, D.V. Dependence of microseism variation periods upon the cyclone propagation velocity and direction. *Dokl. Earth Sci.* **2004**, *394*, 141–144.
12. Dolgikh, G.I.; Chupin, V.A.; Gusev, E.S.; Timoshina, G.A. Cyclonic process of the “voice of the sea” microseism generation and its remote monitoring. *Remote Sens.* **2021**, *13*, 3452. [[CrossRef](#)]
13. Shuleikin, V.V. On Sea Voice. *CR Acad. Sci. USSR* **1935**, *3*, 259.
14. Dolgikh, G.I.; Kovalev, S.N.; Koren', I.A.; Ovcharenko, V.V. A two-coordinate laser strainmeter. *Izvestiya. Phys. Solid Earth* **1998**, *34*, 946–950.
15. Dolgikh, G.I.; Dolgikh, S.G.; Ovcharenko, V.V.; Chupin, V.A.; Shvets, V.A.; Yakovenko, S.V. A laser strainmeter with an accuracy at the level of picometers. *Instrum. Exp. Tech.* **2013**, *2*, 138–139.
16. Dolgikh, G.I. Principles of designing single-coordinate laser strainmeters. *Tech. Phys. Lett.* **2011**, *37*, 204–206. [[CrossRef](#)]
17. Abbott, B.P.; Abbott, R.; Abbott, T.D.; Abernathy, M.R.; Acernese, F.; Ackley, K.; Adams, C.; Adams, T.; Addesso, P.; Adhikari, R.X.; et al. GW151226: Observation of Gravitational Waves from a 22-Solar-Mass Binary Black Hole Coalescence. *Phys. Rev. Lett.* **2016**, *116*, 241103. [[CrossRef](#)] [[PubMed](#)]
18. Earth: A Global Map of Wind, Weather and Ocean Conditions. Available online: <https://earth.nullschool.net> (accessed on 10 September 2022).
19. Bowden, K.F. *Physical Oceanography of Coastal Waters*; Halsted Press: New York, NY, USA, 1983; 302p.

Disclaimer/Publisher’s Note: The statements, opinions and data contained in all publications are solely those of the individual author(s) and contributor(s) and not of MDPI and/or the editor(s). MDPI and/or the editor(s) disclaim responsibility for any injury to people or property resulting from any ideas, methods, instructions or products referred to in the content.